Solar Energy Materials and Solar Cells 169 (2017) 195–202

Contents lists available at ScienceDirect

Solar Energy Materials and Solar Cells

journal homepage: www.elsevier.com/locate/solmat

DLIT- versus ILIT-based efficiency imaging of solar cells

F. Frühauf*, O. Breitenstein

Max Planck Institute of Microstructure Physics, Halle, Germany

ARTICLE INFO

Keywords:
Efficiency imaging
Dark lock-in thermography
Illuminated lock-in thermography
Distributed resistance
Independent diode model

ABSTRACT

Efficiency imaging of solar cells means to know which region of an inhomogeneous cell contributes by which degree to the efficiency at maximum power point of the cell. This knowledge allows us to judge how strong certain defect regions influence the efficiency of the whole cell. Efficiency imaging can be performed based on dark lock-in thermography (DLIT) imaging within the model of independent diodes, or based on illuminated lock-in thermography (ILIT), which does not assume any cell model. Moreover, by 2-dimensional finite element simulation of the cell based on DLIT results, an efficiency image can be obtained, which takes into account the distributed nature of the series resistance. In this contribution these three methods are applied to one and the same multicrystalline cell containing ohmic shunts and the results are compared to each other. Conclusions to the accuracy of solely DLIT-based efficiency imaging are drawn.

1. Introduction

Solar cells, in particular multicrystalline (mc) silicon cells, are inhomogeneous devices. Their bulk lifetime τ, which decisively influences the short circuit current density J_{sc}, the saturation current density J_{01}, and the effective bulk diffusion length L_d, may vary from position to position by an order of magnitude or more [1–4]. For evaluating the influence of certain defect regions on the global cell efficiency it is interesting to know to which degree the different regions in a cell contribute to its efficiency. This task is generally called efficiency imaging. Methods for efficiency imaging of solar cells have been proposed based on dark lock-in thermography (DLIT) imaging ("Local I-V" method, see [2,5]) and based on photoluminescence (PL) imaging [6–8]. All these methods rely on the model of independent diodes. Hence it is assumed there that each elementary cell region (image pixel) is connected to the terminals of the cell by an independent series resistor. It has been shown recently that this clearly too simple model inevitably leads to systematic errors in calculating local currents in inhomogeneous cells from luminescence images after [6,7], since it does not consider the distributed nature of the series resistance [9]. However, it was shown in [9] that saturation current density images obtained by the DLIT-based Local I-V analysis [2] are reliable, in spite of the independent diode model used also there. The reason for this different behavior is that luminescence can only image local diode voltages, and local currents are derived there based on an equivalent circuit (the independent diode model), whereas DLIT is able to image local currents more directly based on local heating. This means that PL-based efficiency imaging after [6,7] is generally not expected to be reliable, in spite of certain improvements [10]. Therefore we have not included PL-based efficiency imaging methods in this work. We also do not consider the PL-based ELBA method [8] in this work, since its efficiency prediction only regards the bulk properties and not any defects of the pn junction, which lead to J_{02}-type and ohmic shunts. Moreover, also these predictions rely on the model of independent diodes, even assuming a constant series resistance [4,8]. On the other hand, even if the J_{01} distribution is imaged correctly by DLIT after [2], the question remains whether the local efficiency analysis after [5] is reliable, since this analysis is based also on the independent diode model.

Already in 2008 Ramspeck et al. have proposed an efficiency imaging method based on illuminated lock-in thermography (ILIT) [11]. This method is based on the fact that the electric power generated by a solar cell and transmitted to an external load reduces the illumination-induced local heating in the cell. Thus, this method is physically very straightforward and does not rely on any equivalent model of the cell. However, in the form published in [11] it only images the internal efficiency for monochromatic illumination, which differs from that for AM 1.5 but can be converted to that, see Section 2. In this work we will propose another variant for evaluating ILIT images leading to the external efficiency for AM 1.5 illumination. Then results of this ILIT-based efficiency imaging should be useful to check the accuracy of DLIT-based efficiency imaging [5], which also predicts the external efficiency at AM 1.5. Most recently a method was proposed to fit a 2-dimensional finite element solar cell model (Griddler [12]) to an

* Corresponding author.
E-mail address: fruehauf@mpi-halle.mpg.de (F. Frühauf).

http://dx.doi.org/10.1016/j.solmat.2017.05.015
Received 28 February 2017; Received in revised form 3 May 2017; Accepted 7 May 2017

existing inhomogeneous cell, mainly relying on DLIT-measured local diode parameters [13]. This method is also based on the local validity of the two-diode model and fully considers the distributed nature of the series resistance. A comparison between this Griddler simulation and the conventional DLIT-based "Local I-V" analysis [5] should allow revealing any inaccuracies in the latter by neglecting the distributed nature of the series resistance. Thus, the goal of this contribution is to cross-check DLIT-based [2,5], ILIT-based [11], and finite element-based [13] local efficiency imaging.

There are two different definitions of a local efficiency, which have been used in parallel in the past. For avoiding any confusion, in the following these two definitions will be described, since both will be used in this work. One definition is the local "in-circuit" efficiency $\eta_{ic}(x,y)$, which is the local contribution of a certain position to the efficiency of the cell, if the cell is at its maximum power point (mpp). Since the terminal voltage under this condition is V_{mpp} and all positions (x,y) contribute to the global cell current by their local diode current density $J_d(x,y)$, the local in-circuit efficiency $\eta_{ic}(x,y)$ is defined as (p_{ill} = illumination power density):

$$\eta_{ic}(x,y) = \frac{J_d(x,y)\,V_{mpp}}{p_{ill}} \tag{1}$$

This definition is independent of any solar cell model. In a two-diode model, the local diode current density can be described as ($J_{sc}(x,y)$ = short circuit current density, $J_{01}(x,y)$ = saturation current density of the first diode, $J_{02}(x,y)$ = saturation current density of the second diode, n_1 = ideality factor of the first diode, n_2 = ideality factor of the second diode, $G_p(x,y)$ = ohmic conductivity (the inverse of the parallel or shunt resistivity R_p), $V_d(x,y)$ = local diode voltage):

$$J_d(x,y) = J_{sc}(x,y) - J_{01}(x,y)\exp\left(\frac{V_d(x,y)}{n_1 V_T}\right) - J_{02}(x,y)\exp\left(\frac{V_d(x,y)}{n_2 V_T}\right) - G_p(x,y)\,V_d(x,y) \tag{2}$$

It has been found regularly by DLIT analyses that both ohmic (G_p) and J_{02} current contributions are always confined to some local positions [2,5,14], see also the results shown here. In these positions the dark current density may easily exceed the photocurrent density (J_{sc}), leading to negative values of J_d. Hence, in these positions the local in-circuit efficiency (1) becomes negative, which means that these positions consume power instead of generating it. Note that V_d in (2) is at mpp usually larger than V_{mpp} and is inhomogeneous due to the series resistance and the inhomogeneity of J_{01}. Note also that (1) defines the so-called external efficiency, since it uses the external illumination intensity as a reference. If instead of this the absorbed illumination intensity is used as a reference, which is reduced by surface reflection and shading, we speak from an internal efficiency, in analogy to external and internal quantum efficiency.

The other definition of a local efficiency is the local efficiency expectation or potential value $\eta_p(x,y)$. This efficiency needs a model description of the cell. In a two-diode model it is calculated from the local diode parameters (J_{01}, J_{sc}, J_{02}, n_2, and G_p), regarding the effective series resistance $R_s(x,y)$ in the model of independent diodes. This definition assumes that the considered position (pixel) is electrically isolated from the neighboring pixels. It is assumed here that this pixel is operating at its individual mpp, which may differ from that of the surrounding pixels. This definition is the usual definition of the efficiency of a solar cell. The physical meaning of the local efficiency potential $\eta_p(x,y)$, as well as the local V_{oc} and fill factor (FF) potentials, is the following: A cell having homogeneously the properties of position (x,y) and a series resistance of R_s is expected to have these values of η, V_{oc}, and FF. In [5] this definition was used for describing the local cell parameters, but in [7] in-circuit values of η, FF, and V_{oc} were reported. The difference between in-circuit and potential values of V_{oc} was pointed out already in [15,16]. As shown there, local $V_{oc}(x,y)$ variations are much larger in the potential representation than in-circuit, with about the same average value. The reason for this difference are horizontal (lateral) balancing currents in the emitter and metallization, which tend to equalize the local diode voltages within the cell. On the other hand, the local efficiency values are generally higher in the potential than in the in-circuit representation, since in the potential representation each pixel is assumed to be at its individual mpp, but in-circuit most of the pixels in an inhomogeneous cell are not. Therefore in-circuit efficiencies may become negative as discussed above, but the efficiency potential is always positive. In the following both definitions will be considered and compared with each other.

In the next Section the physical basics of the three different efficiency imaging methods compared here are briefly summarized. Then Section 3 introduces and compares experimentally obtained efficiency imaging results of the three imaging methods for a mc silicon solar cell containing ohmic shunts. The results are discussed and summarized in Section 4.

2. Description of models and methods

The DLIT based "Local I-V" method was introduced in [2,5] and the "Local I-V 2" software applying this method is available [17]. The method assumes local validity of the two-diode model, hence of the superposition principle (illuminated characteristic = dark characteristic minus short circuit current, holding locally without series resistance) for each position, and it regards R_s as an area-related effective R_s in units of $\Omega\,cm^2$ in the model of independent diodes. The procedure evaluates up to four $-90°$ (out-of-phase) DLIT images, three of them taken at three different forward biases and one at weak reverse bias. Though these $-90°$ images show a limited spatial resolution (depending on the lock-in frequency), they are most appropriate for this quantitative evaluation, since the amplitude images are not additive for different heat sources and contain the in-phase contribution, which only shows information on local heat sources [18]. The software "Local I-V 2" allows the effective series resistance $R_s(x,y)$ to be loaded, $R_s(x,y)$ can be assumed to be homogeneous, or it can be calculated by evaluating an electroluminescence (EL) based local diode voltage image at the highest forward bias together with the corresponding DLIT image according to the so-called RESI method [19], which is implemented in "Local I-V 2". By considering this effective R_s, the procedure first calculates, for each pixel and each bias, the local current densities and the local diode voltages, which deviate from the applied biases due to the influence of R_s. Then the procedure fits all pixels to a two-diode model, leading to the local two-diode parameters J_{01}, J_{02}, n_2, and $G_p = 1/R_p$. By knowing the global short circuit current I_{sc}, the local short circuit current densities $J_{sc}(x,y)$ are modelled within "Local I-V 2" by evaluating the J_{01} distribution according to the method introduced in [20]. Knowing the local two-diode parameters, J_{sc}, and R_s, the procedure now simulates local illuminated characteristics based on the two-diode model with independent diodes for each position. This allows the procedure to calculate for each pixel both local potential values and in-circuit values of V_{oc}, V_{mpp}, J_{mpp}, FF, and the efficiency η, as well as other useful parameters like $J(V_{oc})$ (in-circuit, the average is zero), suns efficiency, suns pFF (both without R_s), and effective ideality factors (of the whole characteristic, not only the J_{02} contribution) in two bias ranges, again with and without the influence of R_s. Finally the software allows to calculate, image, and evaluate dark and illuminated *J-V* characteristics of selected positions, regions, and of the whole cell, both as suns *I-V* characteristics (without R_s) and including the influence of R_s. The evaluation of the whole cell allows the simulation of the global cell parameters V_{oc}, V_{mpp}, J_{mpp}, FF, and η, also with and without the influence of R_s.

The ILIT based local efficiency imaging method after [11] does not rely on any solar cell model. It evaluates two $-90°$ ILIT images, both taken with pulsed illumination, one taken at short circuit and the other at pulsed mpp bias. Simultaneous pulsing of light and bias can be realized electronically or by connecting the cell to an appropriate load

resistor. The basic idea behind this method is the following: As described e.g. in [21], the dissipated power density in an illuminated solar cell at bias V equals the irradiated (absorbed) illumination power density minus the electrically generated and fed-out power density. Hence, at J_{sc} and at V_{oc} condition, where no electric power is generated by the cell, the dissipated power density equals the irradiated power density, and the corresponding ILIT signal can be used as a reference for quantifying the LIT measurements. From these two possibilities the J_{sc}-ILIT signal is better appropriate than the V_{oc}-ILIT one, since under V_{oc} condition substantial amounts of energy are transported laterally within an inhomogeneous cell by the above mentioned horizontal balancing currents. Note that, even if the cell is at J_{sc} condition, the local diodes are not exactly at zero voltage due to the finite R_s. Therefore this method works most accurately for low-R_s cells but may become inaccurate for R_s-dominated cells. In ideal case the difference between the J_{sc}- and the mpp-ILIT image is proportional to the generated electric power density, and the J_{sc}-ILIT signal is proportional to the absorbed light power density. Therefore the internal in-circuit efficiency (not regarding reflectivity) equals [11]:

$$\eta_{ic,int} = \frac{ILIT_{Jsc} - ILIT_{mpp}}{ILIT_{Jsc}} \tag{3}$$

The nominator in (3) should be proportional to the extracted electric power density and the denominator to the total absorbed light intensity. Hence the nominator should allow us to calculate also the external in-circuit efficiency. Then we need the proportionality factor C between ILIT signal and dissipated power density $p = C^{*}ILIT$, which should be the same as for DLIT experiments. Hence C can be calculated by evaluating the cell average of an additional DLIT measurement $< DLIT(V) >$, where bias V and current I for a cell area A are known:

$$C = \frac{IV}{A < DLIT\,(V) >} \tag{4}$$

Alternatively, < DLIT(V) > can be replaced in (4) by the average of the nominator of (3) with $I = I_{mpp}$ and $V = V_{mpp}$. In our case these two values of C differed by only 5%. This leads to the external efficiency:

$$\eta_{ic,ext} = \frac{C\,(ILIT_{sc} - ILIT_{mpp})}{p_{ill}} \tag{5}$$

If here for p_{ill} the AM 1.5 value of 100 mW/cm^2 is inserted and the short circuit current I_{sc} is the nominal value for this cell, Eq. (5) yields the external AM 1.5 efficiency, even if the ILIT measurement is performed monochromatically. The different thermalization losses between monochromatic and AM 1.5 illumination compensate in the difference in the nominator of (5). For lower illumination intensity instead of 100 mW/cm^2, as measured by I_{sc}, a correspondingly lower value of p_{ill} = 100 mW/cm^2*$suns$ ($suns$ = illumination intensity in units of suns) has to be used in (5). Eq. (3) yields, for monochromatic illumination, the internal monochromatic efficiency. This efficiency does not contain the illumination intensity explicitly, since this influences both the nominator and the denominator of (3). The monochromatic efficiency is well above the AM 1.5 efficiency by a constant factor since, for obtaining the same nominal value of J_{sc}, a significantly lower illumination power density is necessary for monochromatic (near-IR) than for AM 1.5 illumination. For calculating this factor we may evaluate the cell average of the J_{sc}-ILIT signal obtained for a nominal value of I_{sc} using C obtained by (4). Regarding that the absorbed power density is the irradiated one multiplied by (1-R) with R being the reflectance (including grid shadowing), this leads for the irradiated monochromatic illumination intensity (before the light hits the cell) to:

$$p_{ill} = \frac{C}{1 - R} < ILIT_{sc} > \tag{6}$$

For converting monochromatic internal efficiencies after (3) to AM 1.5 ones we have to multiply them by a factor of p_{ill}/100 mW/cm^2. Also here, for a monochromatic illumination intensity smaller than 1 sun (equivalent), the factor $suns$ has to be multiplied to the value of 100 mW/cm^2, finally leading with (4) to the AM 1.5 equivalent internal efficiency for reduced illumination intensity of:

$$\eta_{ic,int}^{AM1.5} = \frac{C < ILIT_{Jsc} > (ILIT_{Jsc} - ILIT_{mpp})}{100\frac{mW}{cm^2} suns\,(1 - R)\,ILIT_{Jsc}} \tag{7}$$

For the 850 nm illumination used by us the correction factor between (7) and (3) was found to be 0.649, assuming R = 0.079 (see Section 3.3). This coincides within 9.8% with the monochromatic intensity necessary in a PC1D simulation [22] of an equivalent cell for obtaining the same J_{sc}, related to 100 mW/cm^2 AM 1.5 intensity. Note that the regions of the busbars resp. current rails also contribute to the averages measured in (4) and (6), though there the signal is shadowed. Note also that not all of the radiation, which is not absorbed, is reflected. Some part of it may also be absorbed at the gridlines, which also may lead to errors in estimating p_{ill}. One possible argument against the applicability of this ILIT method to image local efficiency data could also be that, during the mpp-ILIT measurement, the local diodes are at a higher diode voltage than V_{mpp} of the cell due to the voltage drop at R_s. This means that the heat internally dissipated by the current flow across the pn-junction J is slightly larger than $J^{*}V_{mpp}$. This seems to contradict to Eq. (1) where the efficiency is defined based on V_{mpp} of the cell. However, as long as the local $J_{d,mpp}$ is not significantly smaller than J_{sc}, a similar voltage drop is also expected for the J_{sc}-ILIT measurement. Hence the additional amounts of heating in both cases due to the higher than expected diode voltage nearly compensate each other by the subtraction in the nominators of (3) and (5). The same argument has been used to support the validity of ILIT-based J_{sc} imaging, which relies on J_{sc}- and negative bias ILIT [23]. Note also that ILIT-based efficiency imaging is generally not able to predict efficiency potential data, since it does not assume any solar cell model. However, it can be used as a tool for checking the accuracy of DLIT-based efficiency imaging, since it is working under much more realistic (illuminated, mpp) conditions and does not use any of the assumptions and simplifications of "Local I-V", see [2,5]. In particular it does not assume the two-diode model of the cell and the independent diode model.

The Griddler software [12], which is also available [24], is a finite-element method (FEM) solar cell simulation tool, which models the cell plane as a distributed network of resistors and diodes. It is mostly used for optimizing the grid structure of otherwise homogeneous (monocrystalline) solar cells, but can be used also to model inhomogeneous cells. In particular, DLIT-measured distributions of the cell parameters can be implemented, which was demonstrated in [13] and leads to a realistic model of an inhomogeneous solar cell, fully implementing the distributed nature of its series resistance. Within each pixel it uses also a two-diode model. In [13] not only the local diode parameters but also local grid and contact resistances were fitted to the given solar cell, based on the additional evaluation of EL and PL results. However, we have found that, for a well-processed mc cell without serious R_s problems, also the assumption of homogeneous grid and contact resistances leads to a sufficiently realistic description of a multicrystalline cell, if these resistances are realistic and the DLIT-based inhomogeneous cell parameters J_{01}, J_{02}, n_2, and G_p are introduced into the model. This will be done in Section 3.3. where the cell will be modelled at its mpp. Then one of the possible output data are the local values of the diode current density $J_{d,mpp}$(x,y), which allow us to calculate the local external in-circuit efficiency after (1). These data will be compared with that obtained by "Local I-V" and by the ILIT-based external efficiency after (5). The V_{oc} potential predicted by Griddler is about the same as for Local I-V, since the same local diode data are used. The prediction of a local efficiency potential is not meaningful for the Griddler simulation, since, in a two-dimensional resistor network, the assumption of a single effective series resistance for an elementary diode (pixel) is meaningless, see [13,25]. The basic difference between

the Griddler simulation and the Local I-V simulation is that the first takes into account the distributed nature of R_s but the second does not.

3. Results

3.1. Local I-V results

All DLIT and ILIT results shown here are obtained using the "PV-LIT" system of InfraTec (Dresden, Germany [26]) at a lock-in frequency of 10 Hz. The cell temperature was measured from behind by a spring-attached T-sensor and the chuck temperature was regulated for ensuring for all DLIT and ILIT measurements a cell temperature of 25 ± 0.1 °C. The cell bias is provided by a 4-quadrant Höcherl & Hackl NL30V30C16 power supply in 4-wire configuration directly sensing in the middle of the cell. For the DLIT evaluation images at 0.5, 0.55, 0.6, and −1 V have been taken. For obtaining a sufficiently good signal-to-noise ratio the acuisition times have been 60, 60, 30, and 60 min, respectively. The DLIT data in busbar regions, which are shadowed by the contacting current rails, are replaced in this evaluation by averaged data of the surrounding using the "bad pixel correction" option of "Local I-V 2". The local J_{sc} image was simulated in "Local I-V 2" by evaluating the calculated J_{01} image, making use of the flasher value of the global I_{sc}, as described in [20]. This method does not take into account any shadowing. Since about 7.9% of the area is shadowed by the gridlines and the busbars, as it will be shown in Section 3.3., in the present Local I-V evaluation we have increased I_{sc} artificially by 7.9% for ensuring the correct values of J_{sc} in the un-shadowed regions. The local diode voltage image at a bias of 600 mV, which is necessary for calculating the RESI-R_s image within "Local I-V 2", was measured by evaluating EL images of this cell taken at 550 and 600 mV bias by using the "EL-Fit" software, which is available [17], as described in [27]. The EL images were obtained by using a bandpass filter of 950–1000 nm in front of the camera as described in [3], which strongly reduces the influence of photon scatter in the detector, and the resulting diode voltage image was artificially blurred by the thermal PSF for using it in the Local I-V 2 software as described in [13] for preventing artifacts in the J_{01} image. Therefore correcting the EL images for photon scatter in the detector as described in [28] was not necessary for its use in Local I-V. Note that the EL-based measurement of local diode voltages is based on a one-diode model, hence in ohmic shunt regions the results may become inaccurate as will be shown in Section 3.3. Our results will show that, nevertheless, also the ohmic shunt regions will be described fairly well by the DLIT-based methods.

The first task of Local I-V is to separate the local J_{01}-type (bulk and backside recombination), J_{02}-type (depletion region recombination) and ohmic current contributions from each other by evaluating their different voltage dependencies. Fig. 1(a-c) shows these three components. For J_{01} a homogeneous ideality factor of $n_1 = 1$ was assumed. In b) instead of J_{02} the depletion region recombination current density at 600 mV is displayed, since in this evaluation the ideality factor n_2 was considered as variable. The J_{01} current density at this voltage looks very similar as the J_{01} distribution in Fig. 1a) if scaled from 0 to 40 mA/cm^2. Hence, in most of the cell area the J_{01} current dominates, only in the positions of the J_{02}-type shunts the J_{02} current dominates. We see that J_{01} shows local maxima (sometimes called "J_{01}-type shunts" [9]) in the positions of crystal defect regions on a nearly homogeneous background. On the other hand, both the J_{02} current and the ohmic conductance (G_p) are confined to some local positions (J_{02} in some local J_{02}-shunt positions and at the cell edges, ohmic shunts in positions of SiC filaments, see [29,30]). These three distributions are dissimilar, which points to their different physical nature and to the ability of "Local I-V 2" to separate these contributions from each other. These findings are typical for all crystalline silicon solar cells investigated up to now, see also [2,5,14]. Fig. 1f) shows the effective R_s image obtained by evaluating DLIT and EL images according to the RESI method [19]. As it was discussed in [9], this R_s shows local minima in the positions of increased dark current density. This may be considered as an artifact, but it correctly describes the local voltage drops within the simple model of independent diodes used in this evaluation. Since our ILIT setup did only allow for 0.8 suns equivalent illumination intensity (measured by I_{sc} compared to flasher data), all following efficiency simulations assumed 0.8 suns illumination intensity. Fig. 1d) to i) show efficiency-related images simulated by "Local I-V 2". Note that all LIT images used in this work are obtained using the local emissivity correction option provided by the PV-LIT system of InfraTec. Therefore in the DLIT efficiency images the gridlines remain invisible, since they are easily penetrated by the thermal waves. In the ILIT efficiency images the gridlines will become slightly visible since they indeed shade the light and lead to lower local in-circuit efficiencies there. Fig. 1d) and e) show the potential images of η and V_{oc}, and g) and h) show the corresponding in-circuit images of η and V_{oc} at V_{mpp} in the same scaling as for d) and e). We see the predicted differences between these two different representations. In particular the V_{oc} contrast is significantly weaker in-circuit than under the assumption of isolated diodes, see [15,16]. The efficiency potential image in d) indeed shows slightly higher values than the in-circuit efficiency in g). In particular, the efficiency minima in the position of the ohmic shunts go down to only +0.63% in the efficiency potential image d), but reach −82% at the dominant shunt at the top left in the in-circuit efficiency image g). This is demonstrated in Fig. 1i), which shows the same data as in g) scaled from −50 to +20%. The global cell data predicted by "Local I-V 2" will be presented and discussed in Section 4. Remember that all these data refer to an illumination intensity equivalent to 0.8 suns AM 1.5.

3.2. ILIT results

Also these measurement were performed by using the InfraTec PV-LIT system [26] at 10 Hz by using local emissivity correction. The illumination was performed here by a custom-built reflecting light box employing 16 power LED modules Osram SFH 4740, which deliver up to 4.3 W optical power each at peak wavelength of 850 nm. For filtering out the thermal radiation of these LED modules they are placed behind an acrylic window. As mentioned above, the intensity was sufficient for only 0.8 suns equivalent intensity. The custom-built power supply for the LEDs could be pulsed directly by the trigger of the InfraTec PV-LIT system. Also for the ILIT experiments the cell was biased by the Höcherl & Hackl NL30V30C16 power supply for ensuring correct cell bias. Also here the cell temperature was measured from the backside and the base temperature was regulated for all measurements separately to ensure a cell temperature of 25 ± 0.1 °C. Note that, depending on whether electric power is extracted from the cell or not, the heat dissipated by the cell is different. The acquisition time for all ILIT images was 60 min each.

It should be mentioned that we have placed for our DLIT and ILIT measurements a thin woven metal net between cell and metal base for increasing the thermal resistance to this base, as described e.g. in [18,31]. This net has two left-free areas in the positions of the T-sensor and of the backside sense contact. Without using this net, in particular in the J_{sc}-ILIT images, the grooves for distributing the vacuum below the cell became visible as bright regions due to the lower heat conduction to the base there. This effect is most striking in J_{sc}-ILIT since due to the strong uniform heating of the whole cell such inhomogeneities become easily visible. As can be expected, this effect becomes weaker if a higher lock-in frequency is used, but then also the signal-to-noise ratio degrades.

Fig. 2a) shows the J_{sc}-ILIT and b) the mpp-ILIT image taken at pulsed V_{mpp} of this cell of 502 mV, the scaling ranges are indicated. Here the busbars are shadowing the illumination and the current rails shadow any T-modulation below towards the camera. We see that the J_{sc}-ILIT image is indeed very homogeneous, except of the busbar regions. Left and right of the busbars there are extended regions of reduced signal, clearly wider than the width of the current rails. Such

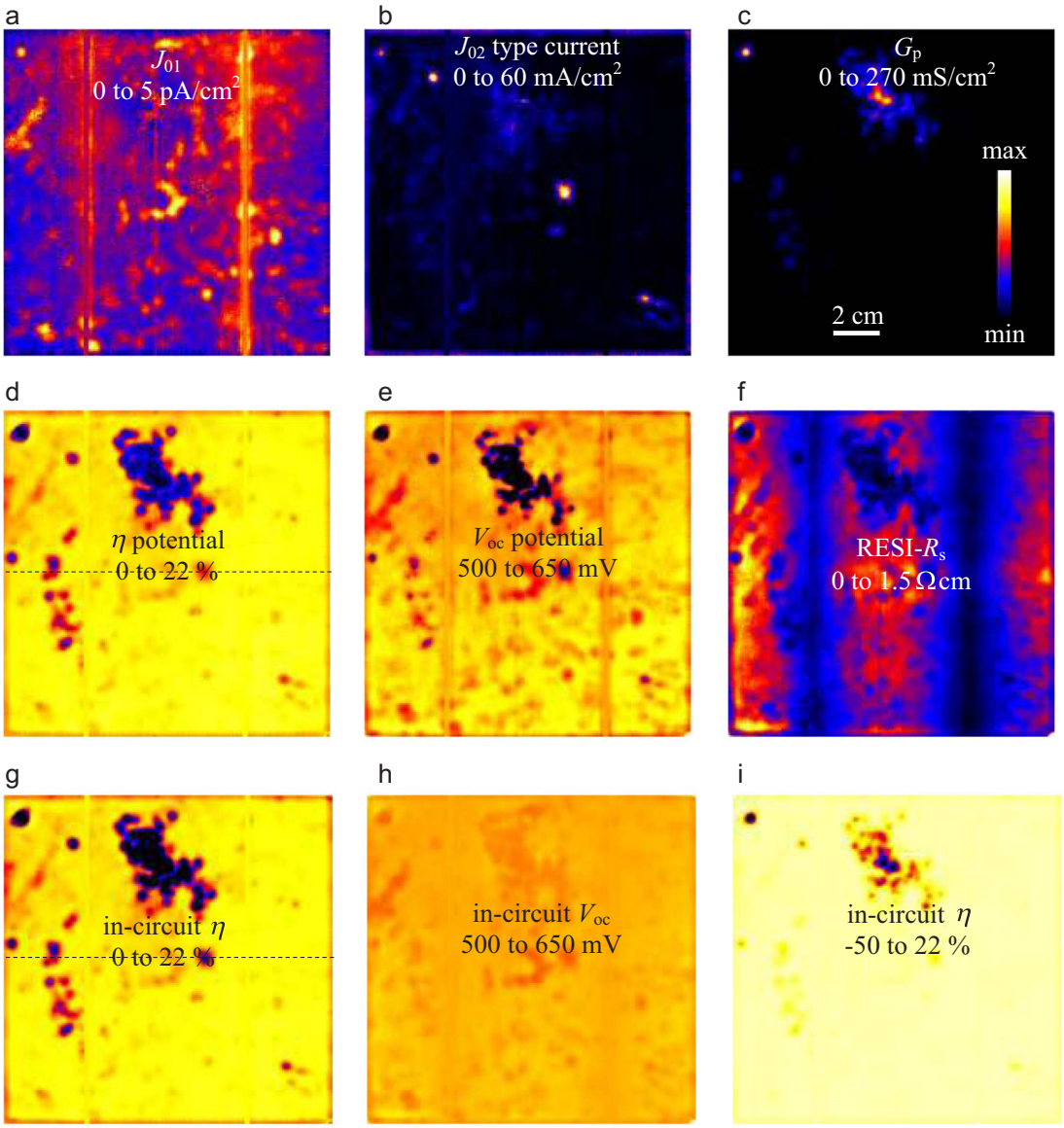

Fig. 1. Local I-V results, a) J_{01}, b) J_{02}-type (depletion region recombination) current density at 600 mV, c) ohmic conductance, d) efficiency potential, e) V_{oc} potential, f) RESI effective R_s, g) in-circuit efficiency, h) in-circuit V_{oc}, i) in-circuit efficiency scaled to negative. The dashed lines in d) and g) mark the position of the linescans that will be shown in Fig. 4.

regions have also been found when a solar cell was investigated, which was completely painted black at the surface. Hence, this is no electronic effect but it comes from the shadowing action of the current rails. Note that our illumination in the reflecting light box is no parallel light perpendicular to the surface, as sunlight is to a high degree, but has strongly inclined components similar to diffuse light. Therefore close to the current rails, which have a height of about 1 cm, the cell is illuminated only from one side, leading to the observed signal reduction there. If highly parallel laser light would be used for illumination, this shadowing effect would be strongly reduced. The two brighter spots in the middle of a) are the positions of the backside potential and thermal sensors, respectively. In the right spot a small crack was present, which leads to a shunt, as visible in the DLIT and efficiency images. Note that this is no ohmic shunt, but, as visible in Fig. 1b), a J_{02}-type shunt. Until now it is not clear why these positions appear bright in the J_{sc}-ILIT image.

Fig. 2c) shows the ILIT-measured external in-circuit AM 1.5 equivalent efficiency after Eq. (7), and d) shows the ILIT-measured internal in-circuit efficiency after Eq. (5) by using the proportionality factor C after (4), both taking into account the illumination intensity of 0.8 suns equivalent. The factor C was obtained based on the 550 mV bias DLIT measurement used for the Local I-V analysis. The ohmic shunts in the upper part of the cell appear only very weakly in the J_{sc}-ILIT image but dominate in the mpp-ILIT image, as expected. As also expected, the rest of the cell shows a lower heating in the mpp-ILIT image than under J_{sc}. The crystal defect regions, which show in Fig. 1a) an increased J_{01}, are invisible in the J_{sc}-ILIT image and appear dark in the mpp-ILIT image, since these regions produce less electric power. The shadowing action of the current rails above the busbars is only visible in the external efficiency image, since this influence of the illumination intensity is compensated in the internal efficiency image. Besides this, the internal and external ILIT-measured efficiency images look quite similar, as expected the average of the internal efficiency is slightly higher than that of the external one. Only in the region around the shunt in T-sensor position, which appeared bright in the J_{sc}-ILIT image Fig. 2a), the external efficiency image shows slightly higher values than the internal efficiency. The reason for this is not clear yet. Generally, the ILIT-measured efficiencies in Fig. 2c) and d) correspond well to the efficiency images in Fig. 1d) and g) measured by DLIT. This proves that these two efficiency imaging methods are basically equivalent. Remaining quantitative differences will be discussed in Section 4.

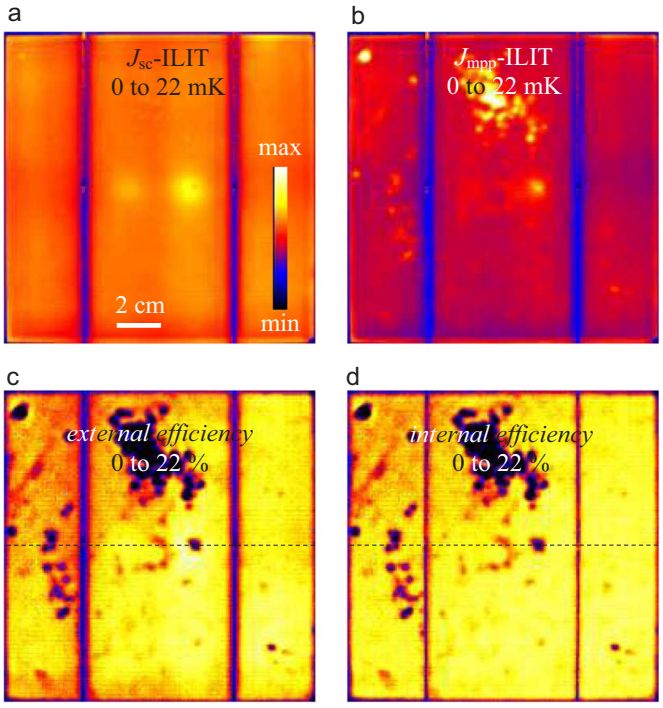

Fig. 2. a) J_{sc}-ILIT image, b) mpp-ILIT image, c) external efficiency, d) internal efficiency, all at 0.8 AM 1.5 equivalent. The dashed lines in c) and d) mark the position of the linescans that will be shown in Fig. 4.

3.3. Griddler results

The DLIT results reported in Section 3.1 are used here to set-up a two-dimensional finite element model of our cell as a network of resistances and diodes, as described in [12,13]. Since Griddler only accepts J_{02} data for $n_2 = 2$, we have converted the Local I-V simulated depletion recombination current density for variable n_2 at a bias of 500 mV, which is close to V_{mpp}, to J_{02} data for $n_2 = 2$. In contrast to [13] the contact and grid resistances are assumed here to be homogeneous across the cell. These two parameters are fitted here for obtaining the best possible fit of the EL-measured local diode voltage image at 600 mV bias to the same image predicted by the Griddler simulation. The result of this fit is a mean contact resistance of 3 mΩcm^2 and a mean grid resistance of 2 mΩ/sqr. Note that the Griddler simulation, in contrast to the Local I-V procedure, considers shadowing of the cell by gridlines and busbars. Therefore we had to multiply the cell-averaged J_{sc}, which is a result of the flasher measurement (here 25.3 mA/cm^2 for 0.8 AM 1.5), by a factor 1/(1-R), with R being the reflectance caused by shadowing, for obtaining J_{sc} in the non-shadowed regions. In particular, we have used the inhomogeneous J_{sc} image predicted by the Local I-V analysis by considering the local bulk recombination after [20] and have multiplied it by the factor mentioned above until the Griddler simulated I_{sc} equals the flasher measured one. This was the case here for $R = 0.079$, hence 7.9% of the area is shadowed. This number is compatible with the gridline width (here 120 μm), the number of gridlines (here 69), and the busbar width (here 2 mm). The same procedure was used already in Section 3.1, for obtaining realistic J_{sc} data in the non-shadowed regions. The main question to be answered by the Griddler simulation was: Does the assumption of an effective local resistance in the model of independent diodes, as made by the Local I-V evaluation method in Section 3.1., lead to significant errors for calculating local in-circuit efficiencies? In this case the local efficiencies calculated by Local I-V and Griddler should deviate significantly.

Fig. 3 shows the main results of the Griddler simulations together with the EL-measured local diode voltage image displayed in Fig. 3a). This local diode voltage image is based on EL images corrected for photon scatter in the detector by spatial deconvolution as described in [3], but the difference to not using deconvolution is very weak due to the bandpass-filtering used here. In the regions of the ohmic shunts the Griddler simulated diode voltages are lying significantly below the EL-measured ones. The reason for this was discussed already in Section 3.1, it is because the EL evaluation uses only a one-diode model, which leads to errors in ohmic shunt regions. We see that the spatial resolution of EL-measured V_d is much better than that of Griddler V_d shown in Fig. 3b). This is because Griddler V_d mainly relies on low-resolution DLIT results. Taking this into account, in most of the non-shunted regions the fit was better than ± 2 mV. This good correspondence proves that the assumption of homogeneous values for the contact and grid resistances is a good approximation here. The Griddler simulated local external efficiency in Fig. 3c) is the local diode current after Eq. (2), which is one of the Griddler simulation results besides the local diode voltage, used in Eq. (1) with $V_{mpp} = 498$ mV (see Section 4) and $p_{ill} = 80$ mW/cm^2 for 0.8 suns AM 1.5 illumination. We see that the Griddler-simulated local efficiency image in Fig. 3c) does not significantly deviate from the Local I-V simulated one in Fig. 1g), apart from the dark gridlines and busbars, which appear only in the Griddler simulation. This proves that, at least in this cell not showing serious series resistance problems, the local efficiency simulations performed by Local I-V may be considered as correct, in spite of the application of the actually too simple model of independent diodes.

4. Summary and conclusions

For enabling a better quantitative comparison of the different local efficiency results reported in this work, Fig. 4 shows linescans of all

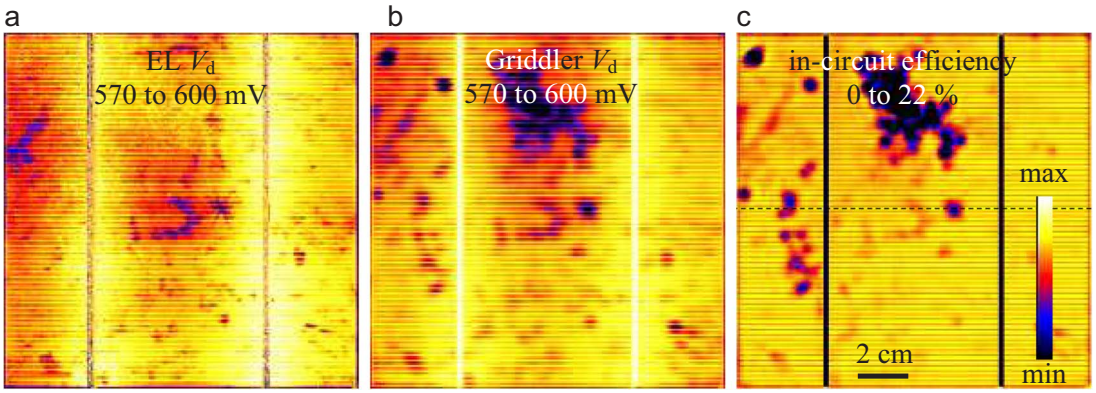

Fig. 3. a) EL-measured local diode voltage at 600 mV bias, b) Griddler simulated local diode voltage at 600 mV bias, c) Griddler simulated in-circuit efficiency (0.8 AM 1.5). The dashed line in c) marks the position of the linescans that will be shown in Fig. 4.

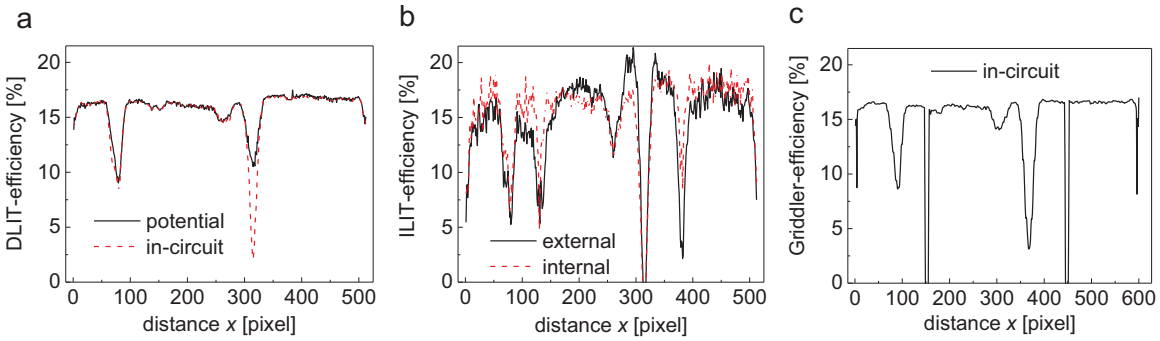

Fig. 4. Linescans of various local efficiency data across the lines indicated in Figs. 1–3. a) DLIT-based η potential and in-circuit η (dashed), b) ILIT-based external and internal η (dashed), c) Griddler-simulated in-circuit η.

these results across the dashed line indicated in Figs. 1–3. Note that this linescan crosses some ohmic shunts at the left, a J_{01}-type shunt in the middle, the J_{02}-type shunt right of it, and the two busbars. We see here, as before in Figs. 1 and 3, that the in-circuit DLIT results in a) are nearly identical to the Griddler-simulated in-circuit results in c), except that the latter also regard shadowing by the busbars. The ILIT-based results in b) also show local minima at these busbars (more blurred, as expected), and they generally show a slightly higher contrast between good and poor regions, which will be discussed below. It is visible that the ILIT-based results show a clearly worse signal-to-noise ratio than the DLIT-based ones. This is mainly due to the fact that the ILIT results rely in the difference between the J_{sc}- and mpp-ILIT images, see Eqs. (3) and (5). Note that the linescan is also lying at the positions of the unexpected local maxima of the J_{sc}-ILIT image in Fig. 2b). In these regions the external ILIT-based efficiency is unexpectedly lying above the internal one.

The comparison of the external in-circuit efficiency images at 0.8 suns of the three efficiency imaging methods compared in this work in Fig. 1g), 2c), and 3c) shows a strong degree of quantitative agreement. This proves that all these methods are appropriate for evaluating the homogeneity of solar cells. Of course, their results are different in some details. For example, the shadowing by gridlines and busbars is considered locally only in the ILIT and Griddler evaluation, but not in the Local I-V evaluation. For obtaining the correct illumination intensity in the regions between the gridlines, the mean value of J_{sc} had to be increased to the nominal one (I_{sc}/A_{cell}) by a factor 1/(1-R) both in the Local I-V and in the Griddler evaluation. While the Griddler evaluation has taken into account the shadowing effects, finally again leading to the correct I_{sc}, Local I-V does not. Hence, if for Local I-V this increased mean J_{sc} is assumed, as it was done in Section 3.1, the local efficiencies between the gridlines appear correctly, but the finally simulated I_{sc} appears too large. Therefore, for the following comparison of the globally predicted efficiencies, the Local I-V evaluation has been repeated by using the nominal mean value of J_{sc}.

Regarding the global cell efficiency predicted by the different methods the agreement is good. The mean value of the ILIT external efficiency in Fig. 2c) is 14.1%, that of the ILIT internal efficiency is 15.2% (is expected to be higher), that of Griddler is 13.9%, and that of Local I-V (using the correct mean value of J_{sc}) is also 13.9%. The flasher-measured efficiency at 0.8 suns is 13.8%, which is most closely to that predicted by Local I-V and Griddler. Obviously, the ILIT-based efficiency imaging method slightly overestimates the mean local efficiencies. Moreover, as mentioned above, the image contrast is slightly higher in the ILIT prediction. While both Local I-V and Griddler predict an efficiency of 16.7% in the best regions and about 13.8% in the position of the J_{01}-type shunt in the middle of the cell, the corresponding values for ILIT are 18.4% and 11.8%. This means that either ILIT somewhat overestimates or DLIT somewhat underestimates the relative influence of local defects. One possible reason for this difference is that the ILIT measurements were performed at a wavelength of 850 nm, whereas for the estimation of the local J_{sc} after [20], which is only low-resolution, the parameters valid for AM 1.5 have been used. Note that also for the ILIT-based efficiency imaging a number of simplifying assumptions hold. It is correct that this method does not assume any cell model, but it assumes, for example, that for an optically homogeneous cell the J_{sc}-ILIT signal is homogeneous. As Fig. 2a) shows, this is not strictly the case. In particular until now we have no clear explanation for the local maximum of the J_{sc}-ILIT signal close to the crack visible in Fig. 3a) right of the J_{01} shunt in the middle of the cell. This maximum is obviously responsible for the higher external than internal ILIT efficiency in this region. One possible explanation could be that, in these positions, the woven metal net below the cell is locally removed. This metal net was introduced for increasing the thermal resistance to the metal base, which was successful for removing the influence of the vacuum grooves below the cell. Hence, it could be expected that the "quasi adiabatic conditions" of lock-in thermography (see [32]) are met already in the regions with the metal net. Therefore the ILIT efficiency results have to be judged with some care. The physical mechanisms underlying ILIT experiments are certainly worth to be investigated in more detail than before. For example, it should be checked whether lateral excess carrier diffusion in the bulk from high lifetime to low lifetime regions could contribute to a higher than expected heat dissipation in low lifetime regions under illumination. This could also explain the somewhat stronger efficiency contrast measured by ILIT.

It can be concluded that the DLIT-based efficiency imaging performed by the Local I-V method [2,5] is obviously realistic and at least delivers a lower limit for the negative influence of local defects on the efficiency of inhomogeneous solar cells. The very good agreement between the Local I-V and the Griddler efficiency simulations have proven that the assumption of the model of independent diodes made in the Local I-V method does not lead to significant errors in predicting local efficiencies. Once an ILIT setup is available, the ILIT based method has the advantage that no other methods and not much modelling are required, it therefore may become easier to perform. If internal efficiencies are sufficient, this method even corrects automatically for inhomogeneous illumination effects. On the other hand, the DLIT-based "Local I-V 2" method enables simple simulations of the influence of illumination intensity and of the quantitative influence of local defect regions. Therefore the ILIT- and DLIT-based methods may supplement each other.

Table 1 summarizes the measured and simulated global cell efficiency parameters obtained in this work. It was explained in Section 2 that the ILIT-based efficiency analysis is performed at a certain mpp but does not lead to the parameters V_{oc} and FF. Again we see a very good agreement between the flasher results and that of the two DLIT-based methods for all global cell parameters.

Table 1
Measured and simulated global cell parameters for the different methods at 0.8 suns.

	Flasher	Local I-V	ILIT	Griddler
external efficiency [%]	13.81	13.9	14.1	13.9
V_{oc} [mV]	597	598	–	596
FF [%	73.18	73.6	–	73.7
J_{mpp} [mA/cm2]	22.2	22.2	22.2	22.3
V_{mpp} [mV]	497	502	498	498

Acknowledgement

The authors are grateful to J. Bauer (MPI Halle) for experimental cooperation and valuable comments. The authors acknowledge the financial support by the German Federal Ministry for Commerce and Energy and by industry partners within the research cluster "SolarLIFE" (contract no. 0325763 D) and InfraTec GmbH [26] for providing and further developing the PV-LIT system used for the DLIT investigations. The content is in the responsibility of the authors.

References

[1] T. Trupke, R.A. Bardos, M.C. Schubert, W. Warta, Photoluminescence imaging of silicon wafers, Appl. Phys. Lett. 89 (2006) 044107.
[2] O. Breitenstein, Nondestructive local analysis of current-voltage characteristics of solar cells by lock-in thermography, Sol. Energy Mater. Sol. Cells 95 (2011) 2933–2936.
[3] O. Breitenstein, F. Frühauf, D. Hinken, K. Bothe, Effective diffusion length and bulk saturation current density imaging in solar cells by spectrally filtered luminescence imaging, IEEE J. Photovolt. 6 (2016) 1243–1254.
[4] O. Breitenstein, F. Frühauf, J. Bauer, F. Schindler, B. Michl, Local solar cell efficiency analysis performed by injection-dependent PL imaging (ELBA) and voltage-dependent lock-in thermography (Local I-V), Energy Procedia 92 (2016) 10–15.
[5] O. Breitenstein, Local efficiency analysis of solar cells based on lock-in thermography, Sol. Energy Mater. Sol. Cells 107 (2012) 381–389.
[6] M. Glatthaar, J. Haunschild, M. Kasemann, J. Giesecke, W. Warta, S. Rein, Spatially resolved determination of dark saturation current and series resistance of silicon solar cells, Phys. Status Solidi RRL 4 (2010) 13–15.
[7] C. Shen, H. Kampwerth, M.A. Green, T. Trupke, J. Carstensen, A. Schütt, Spatially resolved photoluminescence imaging of essential silicon solar cell parameters and comparison with CELLO measurements, Sol. Energy Mater. Sol. Cells 109 (2013) 77–81.
[8] B. Michl, M. Rüdiger, J.A. Giesecke, M. Hermle, W. Warta, M.C. Schubert, Efficiency limiting bulk recombination in multicrystalline silicon solar cells, Sol. Energy Mater. Sol. Cells 98 (2012) 441–447.
[9] O. Breitenstein, J. Bauer, D. Hinken, K. Bothe, The reliability of thermography- and luminescence-based series resistance and saturation current density imaging, Sol. Energy Mater. Sol. Cells 137 (2015) 50–60.
[10] C. Shen, M.A. Green, O. Breitenstein, T. Trupke, M. Zhang, H. Kampwerth, Improved local efficiency imaging via photoluminescence for silicon solar cells, Sol. Energy Mater. Sol. Cells 123 (2014) 41–46.
[11] K. Ramspeck, K. Bothe, J. Schmidt, R. Brendel, Correlation between spatially resolved solar cell efficiency and carrier lifetime of multicrystalline silicon, J. Mater. Sci: Meter Electron. 19 (2008) S4–S8.
[12] J. Wong, Griddler: Intelligent computer aided design of complex solar cells, Proceedings 40th IEEE PVSC, Tampa, pp. 933–938, 2013.
[13] F. Frühauf, J. Wong, J. Bauer, O. Breitenstein, Finite element simulation of inhomogeneous solar cells based on lock-in thermography and luminescence imaging, Sol. Energy Mater. Sol. Cells 162 (2017) 103–113.
[14] O. Breitenstein, J. Bauer, K. Bothe, D. Hinken, J. Müller, W. Kwapil, M.C. Schubert, W. Warta, Can luminescence imaging replace lock-in thermography on solar cells? IEEE J. Photovolt. 1 (2) (2011) 159–167.
[15] C. Shen, H. Kampwerth, M.A. Green, Photoluminescence based open circuit voltage and effective lifetime images re-interpretation for solar cells: the influence of horizontal balancing currents, Sol. Energy Mater. Sol. Cells 130 (2014) 393–396.
[16] O. Breitenstein, C. Shen, H. Kampwerth, M.A. Green, Comparison of DLIT- and PL-based local cell efficiency analysis, Energy Procedia 38 (2013) 2–12.
[17] see ⟨www.maxplanckinnovation.de/en⟩ (March 2017).
[18] O. Breitenstein, W. Warta, M. Langenkamp, Lock-in Thermography - Basics and Use for Evaluating Electronic Devices and Materials, Springer Series in Advanced Microelectronics 10 Springer, Heidelberg, New York, 2010.
[19] K. Ramspeck, K. Bothe, D. Hinken, B. Fisher, J. Schmidt, R. Brendel, Recombination current and series resistance imaging of solar cells by combined luminescence and lock-in thermography, Appl. Phys. Lett. 90 (2007) 153502.
[20] O. Breitenstein, F. Frühauf, M. Turek, Improved empirical method for calculating short circuit current density images of silicon solar cells from saturation current density images and vice versa, Sol. Energy Mater. Sol. Cells 154 (2016) 99–103.
[21] O. Breitenstein, J.P. Rakotoniaina, Electrothermal simulation of a defect in a solar cell, J. Appl. Phys. 97 (2005) 074905.
[22] PC1D, see ⟨https://sourceforge.net/projects/pc1d/⟩ (March, 2017).
[23] F. Fertig, J. Greulich, S. Rein, Spatially resolved determination of the short.circuit current density of silicon solar cells via lock-in thermography, Appl. Phys. Lett. 104 (2014) 201111.
[24] see ⟨http://www.seris.sg/Seris/OurServices/Griddler.html⟩ (March 2017).
[25] F. Frühauf, Y. Sayad, O. Breitenstein, Description of the local series resistance of real solar cells by separate horizontal and vertical components, Sol. Energy Mater. Sol. Cells 154 (2016) 23–34.
[26] see ⟨www.infratec-infrared.com⟩ (March 2017).
[27] O. Breitenstein, A. Khanna, Y. Augarten, J. Bauer, J.-M. Wagner, K. Iwig, Quantitative evaluation of electroluminescence images of solar cells, Phys. Stat. Sol. RRL 1 (2010) 7–9.
[28] O. Breitenstein, F. Frühauf, A. Teal, An improved method to measure the point spread function of cameras used for electro- and photoluminescence imaging of silicon solar cells, IEEE J. Photovolt. 6 (2016) 522–527.
[29] J. Bauer, O. Breitenstein, J.P. Rakotoniaina, Electronic activity of SiC precipitates in multicrystalline solar silicon, Phys. Status Solidi A 204 (2007) 2190–2195.
[30] O. Breitenstein, Understanding the current-voltage characteristic of industrial crystalline silicon solar cells by considering inhomogeneous current distributions, Opto-Electron. Rev. 21 (2013) 259–282.
[31] O. Breitenstein, Lock-in, IR thermography for functional testing of solar cells and electronic devices, QIRT J. 1 (2) (2004) 151–172.
[32] O. Breitenstein, W. Warta, M. Langenkamp, Lock-in Thermography - Basics and Use for Evaluating Electronic Devices and Materials, Second edition, Springer, Heidelberg, 2010.